

# Efficient Light-Field Rendering Using Depth Maps for 100-Mpixel Multi-Projection 3D Display

Young Ju Jeong, Jin-Ho Lee, Yang Ho Cho, Dongkyung Nam, Du-Sik Park, and C.-C. Jay Kuo, *Fellow, IEEE*

**Abstract**—In order to achieve an immersive, natural 3D experience on a large screen, a 100-Mpixel multi-projection 3D display was developed. Ninety-six projectors were used to increase the number of rays emanating from each pixel in the horizontal direction to 96. Conventional algorithms use a large number of cameras or input images to process a large number of light rays. This creates difficulties in the design of both the large acquiring system and substantial memory storage. In this paper, we propose an efficient light-field rendering algorithm that utilizes only a few input colors and depth images. Using a depth map and estimated camera parameters, synthesized light-field images are directly generated. This algorithm requires a much lighter memory load than conventional light-field rendering algorithms. It is also much simpler than the image-based rendering algorithm because it does not require the generation of so many multiview images.

**Index Terms**—Autostereoscopic display, depth image-based rendering, light-field rendering.

## I. INTRODUCTION

**P**ROGRESS in the development of 3D displays has enabled us to reproduce a more realistic 3D world. Stereoscopic displays, introduced in the first developmental stage, offer two stereoscopic images, which provide 3D effects but cannot induce motion parallax. Later multiview displays reproduce a more realistic 3D world with motion parallax by using multiview images. However, this motion parallax can only be experienced when viewed from a certain location. Moreover, accommodation-vergence conflict which is disagreement between the focal point of the eyes and the intersection point of the lines of sight [1] still occurs in multiview displays. It causes eyestrain and discomfort for viewers. Various studies are currently underway to develop 3D displays in order to solve these problems using super multiview displays [2]–[5], tensor displays [6], multi-directional backlight [7], intergral imaging [8], [9], and multi-projection display [10]–[14]. Beyond studies,

Manuscript received March 09, 2015; revised April 28, 2015; accepted April 28, 2015. Date of publication April 30, 2015; date of current version September 08, 2015.

Y. J. Jeong, J.-H. Lee, Y. H. Cho, D. Nam, and D.-S. Park are with the Samsung Advanced Institute of Technology, Suwon, South Korea, and also with the Department of Electrical Engineering, University of Southern California, Los Angeles, CA 90033 USA (e-mail: young.jeong@samsung.com; leejinho@samsung.com; yho.cho@samsung.com; max.nam@samsung.com; dusikpark@samsung.com).

C.-C. J. Kuo is with the Ming-Hsieh Department of Electrical Engineering, University of Southern California, Los Angeles, CA 90089-2564 USA (e-mail: cckuo@sipi.usc.edu).

Color versions of one or more of the figures are available online at <http://ieeexplore.ieee.org>.

Digital Object Identifier 10.1109/JDT.2015.2428281

Holografika has demonstrated and commercialized various multi-projection 3D displays [15], [16].

Panel-based autostereoscopic displays [17]–[19] decrease image resolution by increasing the number of light rays emanating from each pixel. This limits the angle and distance at which 3D images can be clearly viewed. Consequently, changes in parallax images create discontinuity, and natural 3D images cannot be displayed.

A large number of light rays are necessary for the reproduction of realistic 3D displays because, in the real world, we perceive 3D objects based on an abundance of light rays. Light-field displays are good candidates for showing real 3D images without decreasing the image resolution because they reproduce as many light rays as possible. Light-field displays create light rays using a large number of projectors in order to express the 3D world. Consequently, very smooth motion parallax without discontinuity can be acquired, and natural 3D images are obtained without limiting the viewing distance.

### A. Light-Field Rendering

A large number of projectors can improve 3D displays and create a natural 3D world using an abundant light source. However, processing a huge number of light rays is a substantial task. In order to process light-field images, image-based rendering (IBR) algorithms are popular [20], [21]. IBR algorithms do not require geometry. Instead, a collection of sample images is used to render a novel view. In light-field rendering, this collection can be comprised of multiview images, and these multiview images can be obtained using a large number of input camera arrays [22] and a multiview rendering synthesis algorithm [23], [24].

Another technique used to acquire light rays with a light-field rendering algorithm was introduced in [25]–[29]. The authors suggested the use of 2D slices of a 4D function, which does not require a geometric structure. Moreover, its degree of complexity is reasonable because it only selects previously acquired images. However, it requires a large number of input images and, therefore, a substantial amount of memory.

Light-field rendering algorithms which use depth maps, requiring relatively fewer input images and disparity maps were introduced [30], [31]. However they do not generate light-field images using depth maps directly, but generate multiview images then create light-field images by IBR algorithm. Viewpoint-based multiview image processing is sufficient for stereoscopic and multiview displays because these displays produce only a few viewpoint light rays as shown in Fig. 1(a). However the light-field display requires a large number of viewpoints as shown in Fig. 1(b). A substantial number of multiview images

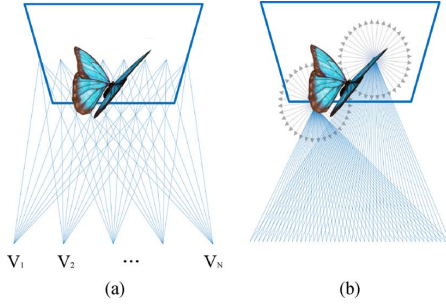


Fig. 1. Light ray configuration of: (a) multiview display and (b) light-field display. The light rays of the multiview display converge to certain points but those of the light-field display do not.

should be generated for the IBR algorithm. As a result, this technique is complex and it needs a large amount of memory storage. Direct light field generation using depth map was introduced by Arachchi *et al.* [32], but it does not contain sufficient information such as specific algorithm process and effects.

This study is an extended version of [33] and [34]. In this study, a 100-Mpixel multi-projection display was developed for medical and educational application. It had a viewing angle of  $24^\circ$  and produced natural 3D video with very smooth motion parallax. We also propose an efficient light-field image generation algorithm based on depth maps, which transforms viewpoint images into the world coordinate structure and maps them to the light-field space.

The rest of this paper is organized as follows. The design for the 100-Mpixel multi-projection 3D display is described in Section II. An efficient light-field rendering that uses depth maps is introduced in Section III. Experimental results are presented in Section IV. Finally, conclusive remarks are given in Section V.

## II. MULTI-PROJECTION 3D DISPLAY

Our 100-Mpixel multi-projection 3D display is composed of multiple projectors, which create the light rays, and a vertical diffuser screen that optically controls projectors' light rays.

### A. Operating Principle

Horizontal parallax only (HPO) light-field displays show images that only have horizontal parallax, and they require a specially designed vertical diffuser screen [10], [11]. Fig. 2 shows the basic configuration and operating principle of the multi-projection 3D display. Numerous projectors are horizontally and vertically arranged in order to produce a large number of light-field rays. Each projector creates a different angle with the screen in order to separate the light-field rays into individual light rays. The screen must compensate for the differences in the vertical positions of the projectors because three-dimensional images only have horizontal parallax. Therefore, the vertical diffuser screen needs to have small horizontal and large vertical diffusion angles. When this vertical diffuser screen is used, an image from one projector is seen as one vertical block. Because two side mirrors are arranged outside of the projectors, the perceived image is composed of 182 vertical light-field blocks from the 96 projectors. Meaning, each block corresponds to the combination of a projected image and its reflection from the side mirrors.

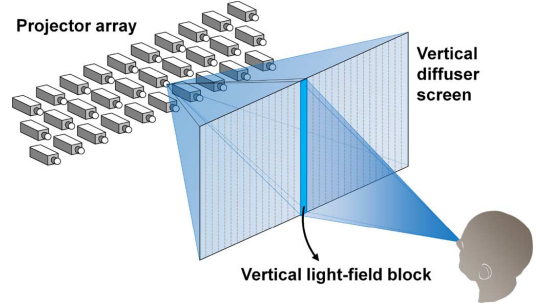


Fig. 2. Basic configuration and operating principle of multi-projection 3D display. The light rays are created using 96 projectors, and a vertical diffuser screen controls the direction of the light ray.

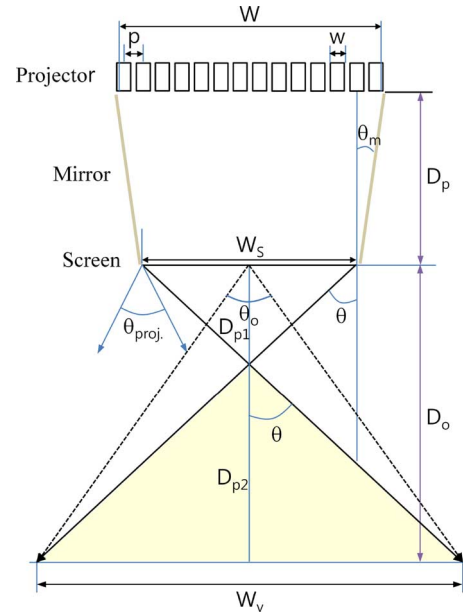


Fig. 3. System design and parameters of multi-projection 3D display, where an overhead view of the basic arrangement of the multi-projection 3D display is shown.

### B. System Design

Fig. 3 shows the overhead view of the basic arrangement of the multi-projection 3D display [35]. The basic layout is determined by the viewing angle  $\theta_o$ , the horizontal length of the screen  $W_s$ , and the total number of projectors  $n$ . Two side mirrors are arranged between the projector array and the screen, and they are slightly tilted to increase the viewing angle. The tilt angle of a mirror  $\theta_m$  and the distance between mirrors near the projector array  $W$  can be calculated using the viewing angle and the horizontal length of the screen. The length of the viewing zone  $W_v$  is expressed by

$$W_v = 2 \times D_o \times \tan\left(\frac{\theta_o}{2}\right) \quad (1)$$

where  $D_o$  denotes the viewing distance. The maximum deflection angle of the light beam  $\theta$  can be calculated by

$$W_s : W_v = D_{p1} : D_{p2} \quad (2)$$

$$\theta = \tan^{-1}\left(\frac{1}{2} \times \frac{W_v}{D_{p2}}\right). \quad (3)$$

The tilt angle of a mirror is expressed by

$$\theta_m = \frac{1}{2} \left( \theta - \frac{1}{2} \theta_{proj} \right) \quad (4)$$

where  $\theta_{proj}$  is the horizontal projection angle of a projector. The distance between mirrors near the projector array is expressed by

$$W = 2 \times D_p \times \tan \theta_m + W_s \quad (5)$$

where  $D_p$  is the projection distance.

The maximum number of projectors in the horizontal direction  $n_h$  is determined by

$$n_h \approx \frac{W}{(w + m)} \quad (6)$$

where  $w$  is width of a projector and  $m$  is a marginal space between projectors. The total number of projectors is represented by

$$n = n_h \times n_v \quad (7)$$

where  $n_v$  is number of projectors in the vertical direction. Since a small  $n_v$  is advantageous for minimizing the keystone effect,  $n_h$  can be determined by the biggest value which satisfy (6) and (7).

### III. DEPTH IMAGE BASED LIGHT-FIELD RENDERING

In this paper, we propose an efficient light-field rendering algorithm that directly generates light-field images using depth maps. On the other hand, the previous algorithms first generate multiview images then render light-field images using the multiview images by IBR algorithm. The amount of image memory required by the proposed algorithm is much smaller than that in IBR-based light-field rendering algorithms. Moreover, the proposed algorithm is much simpler than IBR-based light-field rendering algorithms.

The light-field rendering algorithm is composed of calibration, disparity estimation, 3D modeling, horizontal parallax only rendering, mirror reflection light-field rendering, and consistent hole filling. This study conducts on the light-field rendering by DIBR algorithm.

#### A. Calibration and Disparity Estimation

In order to perform disparity estimation of stereo input contents, the input stereo contents should be rectified so that the matching point of left and right images should locate at the same vertical position [36]. First, we have applied rectification algorithm to stereo contents [37].

Since the field of view of the projection type 3D display is much larger than stereo display, we use wide baseline multiview images. In order to estimate disparity of wide baseline images we first generate down-sampled multiview image, and then apply stereo matching algorithm. The belief propagation algorithm on the simple tree structure is applied to the down-sampled stereo images. Then error region is improved by the depth-color fitting [38]. We generate up-sampled disparity maps using Weighted Mode Filtering [39].

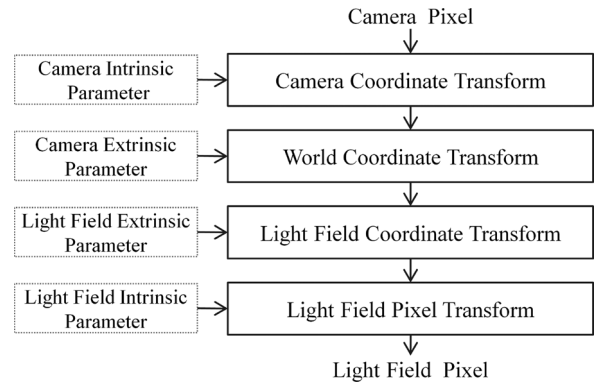


Fig. 4. Block diagram of coordinate transformation from an image pixel to a light-field pixel using DIBR.

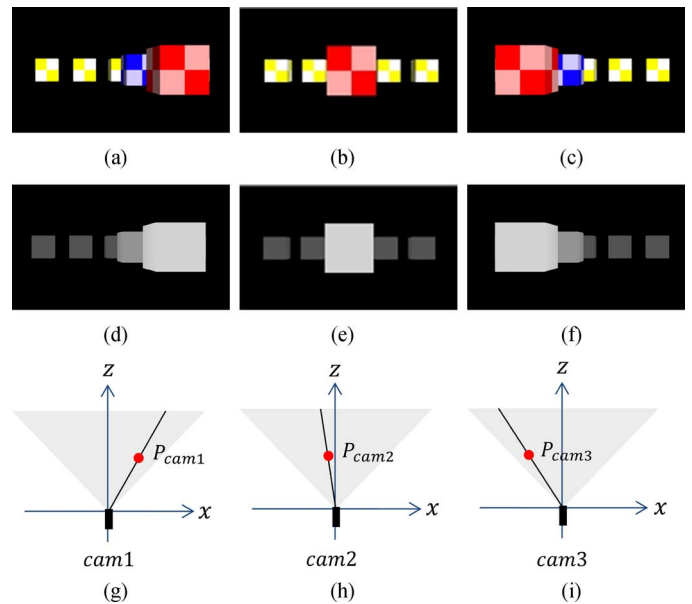


Fig. 5. Input: (a) left color, (b) center color, (c) right color, (d) left depth, (e) center depth, and (f) right depth. The light ray of a given pixel and its geometric depth location of (g) left, (h) center, and (i) right.

#### B. 3D Modeling Using Input Image and Depth

The main idea of light-field 3D rendering using DIBR is to make point clouds from camera-captured images and depth maps. Using color images, a depth map, and camera's configuration, we can infer 3D points that include their color and 3D location information.

Fig. 4 shows a block diagram of coordinate transformation from an image pixel to a light-field pixel using DIBR. Using input camera's intrinsic parameters such as, its pixels are transformed into a camera coordinate system. Then, camera's extrinsic parameters can be used to perform the transformation into a world coordinate system. Using the extrinsic parameters of the projector, the world coordinate system is transposed to a light-field coordinate system. The pixel locations in the light-field image are assigned using the projector intrinsic parameters.

Fig. 5 illustrates input camera images and depth. Given the depth of an image pixel, it can be transformed into a camera coordinate system. A 3D model of the left, center, and right images

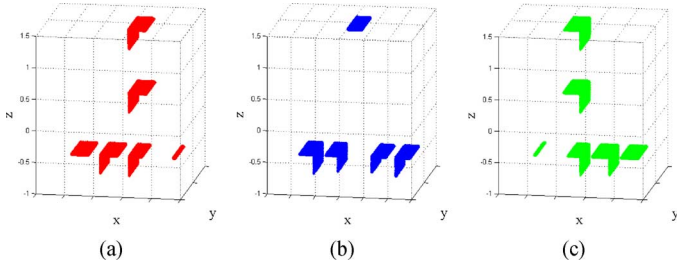


Fig. 6. Three-dimensional points of input color and depth images: (a) the left image, (b) the center image, and (c) the right image.

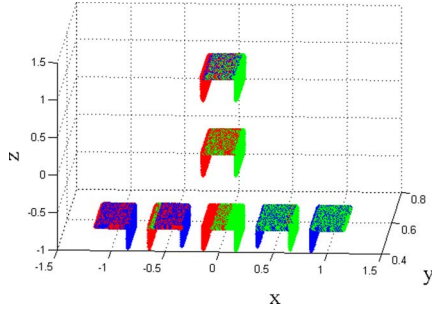


Fig. 7. Three-dimensional points of input color and depth images in the world coordinate system. Red, blue, and green points are shown on the left, center, and right, respectively.

are individually transformed as shown in Fig. 6.  $x$  and  $y$  are the direction of screen width and height, respectively.  $z$  is a direction of viewing location and multi-projection 3D display. The plane at  $z = 0$  is screen plane, and positive  $z$  value means in front of the screen. In the camera coordinate system, perspective geometry distortion does not occur. This means that the cubes shown in Fig. 5 do not have the same metrics as the original cubes but those of the camera coordinate system as given in Fig. 6. The 3D points of each camera can be combined by camera's extrinsic parameters, which are the relative translation and rotation between the cameras. Fig. 7 shows reconstructed 3D points in the world coordinate system. The combined model represents the input image information.

Since the projectors emit light rays with a perspective property, their image can be obtained using the perspective projection of the 3D points given projectors' extrinsic and intrinsic parameters. Extrinsic parameters are given by the design configuration while intrinsic parameters are decided by the projector. There are two differences between the camera and projector projections. The camera selects the nearest point using the occlusion rule. For the projector case, the points farthest from the projector are selected. Additionally, projectors have a keystone factor, which should be considered by intrinsic parameters.

### C. Horizontal Parallax Only Rendering (HPO)

Our display system offers only horizontal parallax through the vertical diffuser screen. Fig. 8 shows HPO rendering, where  $C$  is projector,  $V$  is an object point, and  $B'$  is user location. In the HPO, users should observe the same point  $V$  whether in  $B$  or  $B'$ , regardless of their vertical movement. In order to generate a light ray that is not affected by user's vertical movement,

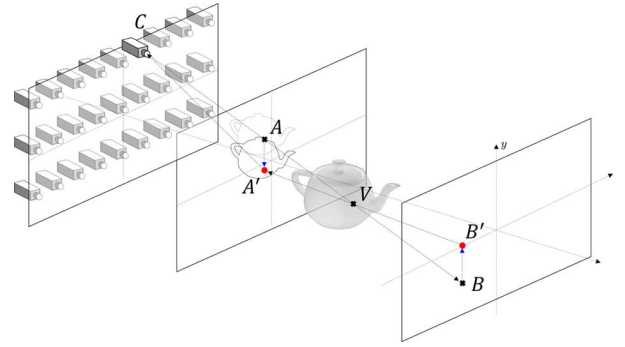


Fig. 8. Projector light rendering for the HPO screen.

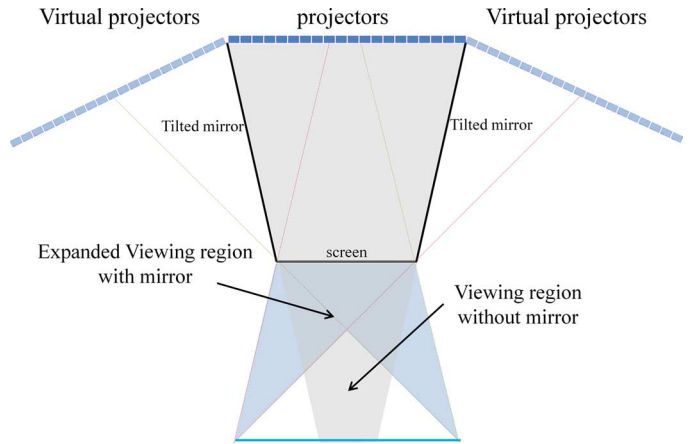


Fig. 9. Real projectors and two tilt mirrors, where real projectors' light rays are reflected from the two tilted mirrors and the reflected light rays act as though they are from virtual projectors.

we should consider the object point point  $V$  as  $A'$  not  $A$ , which is a vertical diffusion point, on the screen plane. With the labelled points  $A'(x'_a, y'_a, z'_a)$ ,  $B'(x'_b, y'_b, z'_b)$ , and  $V(x_v, y_v, z_v)$  in Fig. 8, the applied HPO parameter  $y_v^{HPO}$  can be calculated by

$$y_v^{HPO} = y'_a = \frac{y_v}{z_v - z_b} (-z_b) \quad (8)$$

and this new  $y_v^{HPO}$  is used for the DIBR as world coordinate.

### D. Mirror Reflection Light-Field Rendering

The use of two tilt mirrors for multi-projection 3D display enlarges the viewing angle. Projector arrangement without mirrors generates the gray 3D viewing region as shown in Fig. 9. Light rays of projectors with tilt mirrors expand the viewing region to the blue dashed lines.

In order to generate light-field images for projectors, the reflected light rays should be also considered. The light rays reflected by the mirrors can be considered as if they are produced by the other projectors, which are virtual projectors in Fig. 9. The rotation and translation positions of the virtual projectors are defined using the tilt angle of the mirrors. Using intrinsic and extrinsic parameters, light rays of real and virtual projectors are generated. Then, reflected light rays from the virtual projector and direct light rays from the real projector are combined. Fig. 10 shows images from projectors. The left-side image is

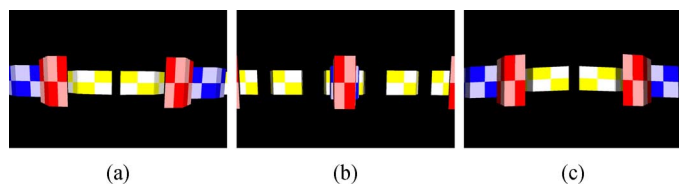


Fig. 10. Projector images: According to the location of projector the portion of image by the real and virtual projector is changed. (a) Leftmost projector. (b) Center projector. (c) Rightmost projector.

from the mirror reflection and the right-side image is from a real projector, in the leftmost projector image in Fig. 10(a). In the rightmost projector image case, the left-side image is from a real projector and the right-side image is from the mirror reflection, in Fig. 10(c). The image of center projector is almost from a real projector, both ends are from the mirror reflection, in Fig. 10(b).

#### E. Consistent Hole Filling

In the process of DIBR, disoccluded hole areas in the synthesized light-field images are created by disparity difference. If the hole area of each light-field image is restored separately, then the same region can be restored with different color. This induces inconsistency of 3D images.

In the consistent hole filling algorithm, we first estimate the largest hole area among the light-field images, then restore the estimated largest hole area. Hole area of each light-field image is filled by the same restored hole information. Recovering the same textures in the hole areas improves view consistency and results in realistic 3D images.

### IV. EXPERIMENTAL RESULTS

#### A. Display System

We designed a 100-Mpixel multi-projection 3D display system with the design parameters listed in Table I. The top image in Fig. 11 shows the 55-inch (1185 × 740 mm, 16:10 aspect ratio) 100-Mpixel multi-projection 3D display system. Ninety-six projectors were attached to the angularly controllable jigs that adjust the tilt angle of the projectors. They were embedded into the frame for the projector arrays as shown at the bottom of Fig. 11. In order to achieve a smaller volume, SCRAM HD-451 projectors (resolution 1,280 × 800 pixels, size 84 × 109.2 × 35 mm) were adopted. A vertical diffuser screen with 1.0° horizontal and 60° vertical diffusion angles was used. Two side mirrors were tilted to 6.62° in order to acquire a 24° viewing angle. The image distribution system was comprised of a controlling personal computer (PC) and two graphics-rendering PCs. Three high-performance ATI FirePro V9000 graphics cards were installed in each graphics-rendering PC, and four outputs of 2560 × 1600-pixel video images were generated by each graphics card. Twenty-four video wall controllers, which divided one 2560 × 1600-pixel image into four 1280 × 800-pixel HD images, were linked between the projectors and graphics cards.

TABLE I  
TARGET SPECIFICATIONS OF MULTI-PROJECTION 3D DISPLAYS

Display Prototype	system
Length of viewing zone at 1.5 m ( $W_v$ )	638 mm
Distance between mirrors near the projector array ( $W$ )	1,641 mm
Tilt angle of a mirror ( $\theta_m$ )	6.62°
Distance from the screen to the imaginary central point $O$	5,106 mm
Horizontal angular pitch between projectors (toward $O$ )	0.138°
Projection distance ( $D_p$ )	1,945 mm
Number of projectors in the vertical direction ( $n_v$ )	6
Number of projectors in the horizontal direction ( $n_h$ )	16
Screen size	55-inch
Viewing Angle	24°
Viewing Distance	1-2 m
Number of Projectors	96
System volume (Optical engine only)	3m <sup>3</sup>
Light-field density	9.6view/IPD
Number of light-field rays	98 M



Fig. 11. The 55-in, 100-Mpixel multi-projection 3D display system.

#### B. Comparison Results of DIBR and IBR

IBR light-field rendering algorithm generates multiview images first. Then projector images can be created by IBR technique which selects and assigns suitable pixel among multiview images to the projector image pixel location. Since IBR algorithm does not need depth structure, sufficient multiview images are required to present natural light rays. In this experiment we use 20, 100, and 500 multiview images for the IBR algorithm in order to compare DIBR and IBR algorithm quality.

To compare light-field images for DIBR and IBR, we used three computer graphic input images and three input depths. The screen was located at  $z = 0$  m, the three cameras were located at  $z = 1.65$  m. The cameras were separated by 0.6 m and the total baseline of three cameras was 1.20 m. Intrinsic parameters for each camera and  $z$ -values for each image were available.

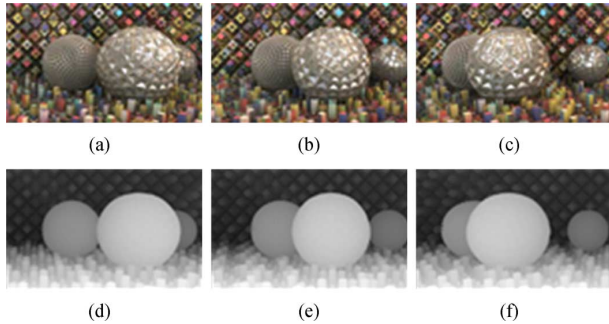


Fig. 12. Input: (a) left color, (b) center color, (c) right color, (d) left depth, (e) center depth, and (f) right depth.

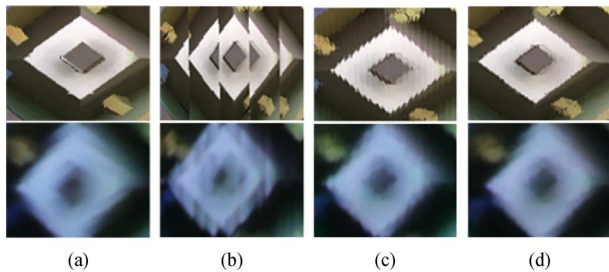


Fig. 13. Magnified particle images of synthesized projector images (upper row) and displayed 3D images captured by camera (lower row): (a) rendered by DIBR algorithm, (b)–(d) rendered by the IBR algorithm using: 20 (b), 100 (c), and 500 (d) multiview images.

Fig. 12 shows the input colors and depth maps, (a) is left image, (b) is center image, and (c) is right image.

Fig. 13 shows magnified particle images of synthesized projector image (upper row) and displayed 3D image which is captured by camera (lower row). Fig. 13(a) is the result of our proposed algorithm which is DIBR, and Fig. 13(b)–(d) are results of the previous algorithm which is IBR; Fig. 13(b) was generated from 20 images, Fig. 13(c) was generated from 100 images, and Fig. 13(d) was generated from 500 images. Fig. 13(a) does not contain quantization artifacts because proposed algorithm generates projector images using depth structure. However the IBR images have quantization artifacts up to 100 images. Quantization artifacts were absent only when a sufficient number of input images, such as 500 images, were provided. As shown in the lower images of Fig. 13(b) and (c), these quantization artifacts appeared in the 3D display, too. As a result, we acquired the similar image quality of 500 images IBR with proposed DIBR method with very small burden of image generation.

DIBR algorithm is more efficient than IBR algorithm in the aspect of computation time and memory usage. Tables II and III demonstrate computation time and memory usage comparison between DIBR method and IBR method under Inter Xeon CPU @3.07 GHz processor. The computation time and memory usage are less than previous method because DIBR does not need time and memory for the multiview image generation. On the other hand, IBR algorithm requires more computation time and memory usage according to the increasing number of multiview images.

Fig. 14 presents displayed 3D images in our light-field display; (a) shows a left-sided image, (b) shows a center view point image, and (c) shows a right-sided image. Light-field for the

TABLE II  
COMPUTATION TIME COMPARISON (SEC)

DIBR (proposed)	IBR (20 multiview)	IBR (100 multiview)	IBR (500 multiview)
7.26	12.23	12.82	15.78

TABLE III  
MEMORY USAGE COMPARISON (MEGA BYTE)

DIBR (proposed)	IBR (20 multiview)	IBR (100 multiview)	IBR (500 multiview)
288	342	558	1638

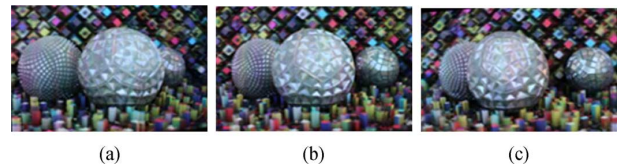


Fig. 14. Displayed 3D images from multi-projection 3D display: (a) left image, (b) center image, (c) right image.

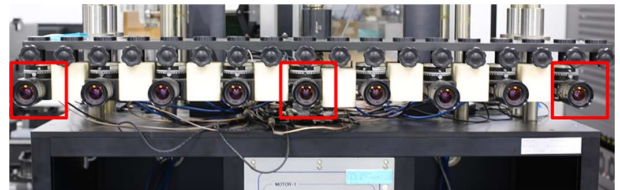


Fig. 15. Multi-camera capturing system: each camera is separated by 130 mm. Cameras indicated by red rectangle (1st, 5th, and 9th cameras) are used for the input images.

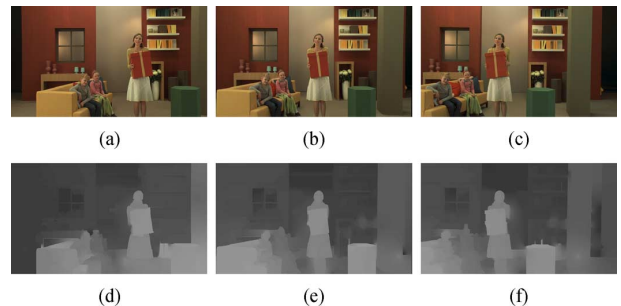


Fig. 16. Input colors and estimated disparity maps (a) from first camera image, (b) fifth camera image, (c) ninth camera image, (d) estimated disparity of first camera image, (e) estimated disparity of fifth camera image, and (f) estimated disparity of ninth camera image.

projection type 3D display is well created by DIBR algorithm, providing large motion parallax.

### C. Results of Camera Captured Contents

To generate light-field image from real life contents, we made the multiview camera capturing system, and took real life multiview contents. We use only three view images for the input to reduce processing complexity, and then generate 100-Mpixel light-fields for the multi-projection 3D display.

Fig. 15 shows multi-camera capturing system. The camera model is FUJINON Corporation CF12.5HA-1 with 54.13° field of view. The cameras are separated by 130 mm for each. Among

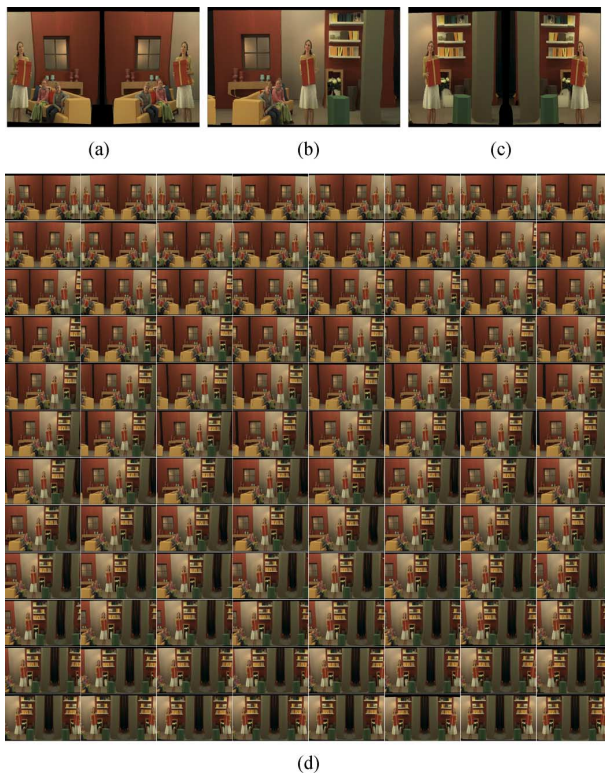


Fig. 17. Light-field images for projectors. (a) Image of projector 1. (b) Image of projector 48. (c) Image of projector 96. (d) Images for 96 projectors.

cameras we use only three camera input images, leftmost, center, and rightmost cameras.

Fig. 16 shows captured input stereo colors and estimated disparity maps. To create large motion parallax, we captured scene with sufficient baseline between cameras. However there is tradeoff between disparity estimation and large motion parallax. If the baseline is large then the disparity value between input images becomes big, yielding difficulties in the disparity estimation process. In order to overcome the difficulties of disparity estimation, we use down-sampled input image for disparity estimation. The disparity maps of Fig. 16 shows artifacts in the texture less region. However the error of the texture less region does not deteriorate the rendered images.

Fig. 17 demonstrates the light-field images for the 96 projectors. Since projectors are located from left to right, the woman in the figure is close to the window in the left projector images and the woman is close to the bookshelf in the right projector images.

## V. CONCLUSION

We have implemented and verified DIBR light-field rendering algorithm through the multi-projection 3D display. In order to process 100-Mpixel light rays, we proposed an efficient light-field rendering algorithm that uses relatively fewer input images and depth maps. As demonstrated by experimental results, our proposed algorithm performs better than conventional IBR algorithms in terms of memory, complexity, and quality.

## REFERENCES

- [1] T. Inoue and H. Ohzu, "Accommodative responses to stereoscopic three-dimensional display," *Appl. Opt.*, vol. 36, no. 19, pp. 4509–4515, 1997.
- [2] Y. Takaki, "Super multi-view display with 128 viewpoints and view-point formation," *IS&T/SPIE Electron. Imaging*, vol. 7237, 2009, Art. ID 72371T.
- [3] H. Nakanuma, H. Kamei, and Y. Takaki, "Natural 3D display with 128 directional images used for human-engineering evaluation," *Electron. Imaging*, pp. 28–35, 2005.
- [4] Y. Takaki and N. Nago, "Multi-projection of lenticular displays to construct a 256-view super multi-view display," *Opt. Exp.*, vol. 18, no. 9, pp. 8824–8835, 2010.
- [5] Y. Takaki, "Thin-type natural three-dimensional display with 72 directional images," *Electron. Imaging*, pp. 56–63, 2005.
- [6] G. Wetzstein, D. Lanman, M. Hirsch, and R. Raskar, "Tensor displays: Compressive light field synthesis using multilayer displays with directional backlighting," *ACM Trans. Graph.*, vol. 31, no. 80, pp. 1–11, 2012.
- [7] D. Fattal, Z. Peng, T. Tran, S. Vo, M. Fiorentino, J. Brug, and R. G. Beusoleil, "A multi-directional backlight for a wide-angle, glasses-free three-dimensional display," *Nature*, vol. 495, no. 7441, pp. 348–351, 2013.
- [8] O. H. Willemssen, S. T. Zwart, M. G. Hiddink, D. K. Boer, and M. P. Krijn, "Multi-view 3D displays," in *SID Symp. Dig. Tech. Papers*, 2007, vol. 38, pp. 1154–1157, 1.
- [9] T. Ito, "Future television—super hi-vision and beyond," in *Proc. IEEE Asian Solid State Circuits Conf.*, 2010, pp. 1–4.
- [10] M. Kawakita, S. Iwasawa, M. Sakai, Y. Haino, M. Sato, and N. Inoue, "3D image quality of 200-inch glasses-free 3D display system," *IS&T/SPIE Electron. Imaging*, vol. 8288, 2012, Art. ID 82880B.
- [11] T. Balogh, "The holovizio system," *Electron. Imaging*, 2006.
- [12] K. Kikuta and Y. Takaki, "Development of SVGA resolution 128-directional display," *Electron. Imaging*, vol. 6055, 2006, Art. ID 60550U.
- [13] K. Nagano, A. Jones, J. Liu, J. Busch, X. Yu, M. Bolas, and P. Debevec, "An autostereoscopic projector array optimized for 3D facial display," *ACM SIGGRAPH Emerging Technol.*, no. 3, 2013.
- [14] J. Jurik, A. Jones, M. Bolas, and P. Debevec, "Prototyping a light field display involving direct observation of a video projector array," in *Proc. IEEE Comput. Soc. Conf. Comput. Vis. Pattern Recogn. Workshops*, 2011, pp. 15–20.
- [15] T. Balogh, "Method and apparatus for displaying 3D Images," U.S. Patent 6999 071, Feb. 14, 2006.
- [16] T. Balogh, "Method and apparatus for generating 3D images," U.S. Patent 7959 294, Jun. 14, 2011.
- [17] N. A. Dodgson, "Analysis of the viewing zone of multiview autostereoscopic displays," *Proc. SPIE Stereosc. Displays and Virtual Reality Syst.*, vol. 4660, pp. 254–265, 2002.
- [18] C. N. De Boer, R. Verleur, A. Heuvelman, and I. Heynderickx, "Added value of an autostereoscopic multiview 3-d display for advertising in a public environment," *Displays*, vol. 31, no. 1, pp. 1–8, 2010.
- [19] F. Okano, "3D TV with integral imaging," in *Proc. SPIE Defense and Security Symp.*, 2008, vol. 6983, Art. ID 69830N.
- [20] H.-Y. Shum, S.-C. Chan, and S. B. Kang, *Image-Based Rendering*. New York, NY, USA: Springer-Verlag, 2006.
- [21] A. M. Siu and R. W. Lau, "Image registration for image-based rendering," *IEEE Trans. Image Process.*, vol. 14, no. 2, pp. 241–252, Feb. 2005.
- [22] B. Wilburn, N. Joshi, V. Vaish, M. Levoy, and M. Horowitz, "High-speed videography using a dense camera array," in *Proc. IEEE Comput. Soc. Conf. Comput. Vis. Pattern Recogn.*, 2004, vol. 2, pp. 294–301.
- [23] C. Fehn, "Depth-image-based rendering (DIBR), compression, and transmission for a new approach on 3D-TV," *Proc. SPIE Stereoscopic Displays and Virtual Reality Syst.*, vol. 5291, pp. 93–104, 2004.
- [24] A. Smolic, K. Muller, K. Dix, P. Merkle, P. Kauff, and T. Wiegand, "Intermediate view interpolation based on multiview video plus depth for advanced 3D video systems," in *Proc. 15th IEEE Int. Conf. Image Process.*, 2008, pp. 2448–2451.
- [25] M. Levoy and P. Hanrahan, "Light field rendering," in *Proc. 23rd Annu. Conf. Comput. Graphics and Interactive Techn.*, 1996, pp. 31–42.
- [26] S. J. Gortler, R. Grzeszczuk, R. Szeliski, and M. F. Cohen, "The lumigraph," in *Proc. 23rd Annu. Conf. Comput. Graphics and Interactive Techn.*, 1996, pp. 43–54.
- [27] M. Levoy, "Light fields and computational imaging," *IEEE Computer*, vol. 39, no. 8, pp. 46–55, 2006.

- [28] E. H. Adelson and J. R. Bergen, "The plenoptic function and the elements of early vision," *Computational Models of Visual Processing*, vol. 1, no. 2, pp. 3–20, 1991.
- [29] L. McMillan and G. Bishop, "Plenoptic modeling: An image-based rendering system," in *Proc. 22nd Annu. Conf. Comput. Graphics and Interactive Techn.*, 1995, pp. 39–46.
- [30] T. Balogh, Z. Nagy, P. T. Kovács, and V. K. Adhikarla, "Natural 3D content on glasses-free light-field 3D cinema," *IS&T/SPIE Electron. Imaging*, vol. 8648, 2013.
- [31] A. Ouazan, P. T. Kovacs, T. Balogh, and A. Barsi, "Rendering multi-view plus depth data on light-field displays," in *Proc. 3DTV Conf.: The True Vision-Capture, Transmission and Display of 3D Video*, 2011, pp. 1–4.
- [32] H. K. Arachchi *et al.*, "D3.6 Report on 3D Audio/Video Rendering and Content Adaptation," DIOMEDES, European Commission WP3, 2011.
- [33] J.-H. Lee, Y. Kim, J. Park, D. Nam, and D.-S. Park, "Design and calibration of 100-Mpixel multi-projection 3D display with an enhanced image quality," in *SID Symp. Dig. Tech. Papers*, 2014, vol. 45, pp. 520–523, 1.
- [34] Y. J. Jeong, J. Y. Park, J.-H. Lee, D. Nam, and C.-C. J. Kuo, "Efficient light-field rendering using depth maps," in *SID Symp. Dig. Tech. Papers*, 2014, vol. 45, pp. 877–880, 1.
- [35] J.-H. Lee, J. Park, D. Nam, S. Y. Choi, D.-S. Park, and C. Y. Kim, "Optimal projector configuration design for 300-Mpixel multi-projection 3D display," *Opt. Exp.*, vol. 21, no. 22, pp. 26820–26835, 2013.
- [36] D. Scharstein and R. Szeliski, "A taxonomy and evaluation of dense two-frame stereo correspondence algorithms," *Int. J. Comput. Vis.*, vol. 47, no. 1–3, pp. 7–42, 2002.
- [37] A. Fusiello and L. Irsara, "Quasi-euclidean uncalibrated epipolar rectification," in *Proc. 19th Int. Conf. Pattern Recogn.*, 2008, pp. 1–4.
- [38] Y. J. Jeong, J. Kim, H. Y. Lee, and D.-S. Park, "Confidence stereo matching using complementary tree structures and global depth-color fitting," in *Proc. IEEE Int. Conf. Consumer Electron.*, 2013, pp. 468–469.
- [39] D. Min, J. Lu, and M. N. Do, "Depth video enhancement based on Weighted Mode Filtering," *IEEE Trans. Image Process.*, vol. 21, no. 3, pp. 1176–1190, Mar. 2012.



displays. Her research interests include 3D vision and 3D lightfield rendering.

**Young Ju Jeong** received the B.S. degree in electrical engineering from Korea University, Seoul, South Korea, in 2005, and the M.S. degree in electrical engineering from the University of Southern California, Los Angeles, USA, in 2007, where she is currently working toward the Ph.D. degree in electrical engineering.

She is currently a Research Member with the Samsung Advanced Institute of Technology, Suwon, South Korea. She has been working on computer vision and image processing for autostereoscopic displays. Her research interests include 3D vision and 3D lightfield rendering.



Korea. His research interest includes the design and fabrication of 3D display, laser display and optical micro devices.

**Jin-Ho Lee** received the B.S. degree in metallurgical engineering from Hanyang University, Seoul, Korea, in 1989, the M.S. degree in materials science and engineering from Pohang University of Science and Technology, Pohang, Korea, in 1991, and the Ph.D. degree in materials science and engineering from Korea Advanced Institute of Science and Technology, Daejeon, Korea, in 2003.

Since 1992, he has been a Member of Research Staff with Samsung Advanced Institute of Technology, Samsung Electronics Co. Ltd., Suwon,



**Yang Ho Cho** received the B.S., M.S., and Ph.D. degrees in electronic engineering from Kyungpook National University, Daegu, Korea, in 2000, 2002, and 2006, respectively.

He joined Samsung Advanced Institute of Technology, Suwon, Korea, in 2006, where he is an R&D Staff Member. His research interests include color image processing, super resolution, multi-view synthesis, and 3D video processing.



**Dongkyoung Nam** received the B.S. and M.S. degrees from Seoul National University, Seoul, Korea, in 1994 and 1996, respectively, and the Ph.D. degree from Korea Advanced Institute of Science and Technology, Daejeon, Korea, in 2002, all in electrical engineering.

He is currently a Senior Researcher working in the field of video processing and 3D display technologies at Samsung Advanced Institute of Technology, Samsung Electronics, Suwon, Korea.



perception.

Mr. Park was the recipient of the Silver Tower Order of Industrial Service Merit by the Korean Intellectual Property Office in 2008, SID Distinguished Paper Award in 2010, IMID Outstanding Poster Paper Award in 2011, and ICCE Best Oral Paper Award in 2012. He was the recipient of an Honorary Doctorate as a special award from Samsung Electronics in 2010.

**Du Sik Park** received the B.S. degree in electronic engineering from Yeungnam University, Gyeongsan, Korea, in 1991, and the M.S. degree in information technology from Pohang University of Science and Technology, Pohang, Korea, in 2000.

He has worked for Samsung Advanced Institute of Technology, Samsung Electronics, Kiheung, Korea since 1991, where he is currently a Vice President and Director of Multimedia Processing Lab. His major fields of research include color imaging, image and video processing, 3D video processing, human visual



From October 1987 to December 1988, he was a Computational and Applied Mathematics Research Assistant Professor with the Department of Mathematics, University of California, Los Angeles, CA, USA. Since January 1989, he has been with the University of Southern California, Los Angeles, where he is presently Director of the Multimedia Communication Laboratory and a Professor of electrical engineering and computer science. He is the coauthor of approximately 220 journal papers, 850 conference papers, and 12 books. His research interests are in the areas of multimedia data compression, communication and networking, multimedia content analysis and modeling, and information forensics and security.

Dr. Kuo is listed as the top advisor in the Mathematics Genealogy Project with 120 supervised Ph.D. alumni.

**C.-C. Jay Kuo** (S'83–M'86–SM'92–F'99) received the B.S. degree from the National Taiwan University, Taipei, Taiwan, in 1980, and the M.S. and Ph.D. degrees from the Massachusetts Institute of Technology, Cambridge, MA, USA, in 1985 and 1987, respectively, all in electrical engineering.